BEILSTEIN JOURNAL OF NANOTECHNOLOGY

Exploring the photoleakage current and photoinduced negative bias instability in amorphous InGaZnO thin-film transistors with various active layer thicknesses

Dapeng Wang[*1] and Mamoru Furuta[*2,3]

Full Research Paper

Open Access

Address:
[1]Key Laboratory of Applied Surface and Colloid Chemistry, Ministry of Education; Shaanxi Key Laboratory for Advanced Energy Devices; Shaanxi Engineering Lab for Advanced Energy Technology, School of Materials Science and Engineering, Shaanxi Normal University, Xi'an 710119, China, [2]School of Environmental Science and Engineering, Kochi University of Technology, Kami, Kochi 782-8502, Japan and [3]Center for Nanotechnology in Research Institute, Kochi University of Technology, Kami, Kochi 782-8502, Japan

Email:
Dapeng Wang[*] - dpwang@snnu.edu.cn; Mamoru Furuta[*] - furuta.mamoru@kochi-tech.ac.jp

* Corresponding author

Keywords:
active layer thickness; gate bias; illumination stress; InGaZnO; photoleakage current; thin-film transistors

Beilstein J. Nanotechnol. **2018,** *9,* 2573–2580.
doi:10.3762/bjnano.9.239

Received: 09 May 2018
Accepted: 07 September 2018
Published: 26 September 2018

Associate Editor: E. Meyer

© 2018 Wang and Furuta; licensee Beilstein-Institut.
License and terms: see end of document.

Abstract

The photoleakage current and the negative bias and illumination stress (NBIS)-induced instability in amorphous InGaZnO thin-film transistors (a-IGZO TFTs) with various active layer thicknesses (T_{IGZO}) were investigated. The photoleakage current was found to gradually increase in a-IGZO TFTs irrespective of the T_{IGZO} when the photon energy of visible light irradiation exceeded ≈2.7 eV. Furthermore, the influence of the T_{IGZO} on NBIS-induced instability in a-IGZO TFTs was explored by the combination of current–voltage measurements in double-sweeping V_{GS} mode and capacitance–voltage measurements. The NBIS-induced hysteresis was quantitatively analyzed using a positive gate pulse mode. When the T_{IGZO} was close to the Debye length, the trapped electrons at the etch-stopper/IGZO interface, the trapped holes at the IGZO/gate insulator interface, and the generation of donor-like states in an a-IGZO layer were especially prominent during NBIS.

Introduction

Over the last decade, the amorphous oxide-based semiconductor thin-film transistors (AOS TFTs) have attracted global attention for use in advanced display technologies due to their outstanding properties such as high electron mobility, good transparency to visible light, and low process temperature with good uniformity [1-4]. Among the numerous AOS materials, indium gallium zinc oxide (IGZO) is one of the most promising candidates used as the active layer because of its excellent electrical and optical properties [5-8]. Although the band gap of IGZO (≈3.1 eV) is higher than the photon energy of visible light, pho-

toinduced leakage current under visible-light irradiation can be detected in the oxide-based TFTs [9,10]. This is due to the fact that the electrons are excited from the trapped states existing near the valence band (E_V). In addition, the a-IGZO TFTs inevitably suffer electrical and optical stresses during practical operation conditions, especially for the negative bias and illumination stress (NBIS) tests [11-16], which leads to device instability and restricts the development of oxide TFTs for commercial products.

In our previous study, a double-sweeping V_{GS} mode was proposed to investigate the origin of NBIS-induced hysteresis of a-IGZO TFTs [17]. A promising method to suppress NBIS degradation was also considered by applying a large negative V_{DS} bias of $V_{DS} < V_{GS}$ during NBIS [18]. These studies imply that the fabrication parameters for the active layer should be well taken into account to improve the reliability of oxide TFTs. The active layer thickness is a key parameter to modify the performance of a-IGZO TFTs. Some works have highlighted that the electrical properties of the device (for both the initial and after stress conditions) such as threshold voltage, on/off ratio, and field effect mobility, can be effectively adjusted by controlling the active layer thickness [19-23]. Up to now, the impact of the active layer thickness (T_{IGZO}) on the photoleakage current and NBIS-induced instability in a-IGZO TFTs has been rarely reported. The NBIS-induced degradation of a-IGZO TFTs with various active layer thicknesses has also rarely been discussed.

In this study, a-IGZO films with various active layer thicknesses were prepared by magnetron sputtering. The initial electrical properties and the photoleakage current of a-IGZO TFTs with various active layer thicknesses were investigated. The subthreshold value slightly increased while the threshold voltage (V_{th}) and mobility (μ) decreased with increasing T_{IGZO}. The photoleakage current increased in all TFTs when the wavelength of visible-light irradiation was shorter than 460 nm. Moreover, the photoleakage current increased with an increase in the T_{IGZO}. Furthermore, the impact of the active layer thickness on the NBIS-induced instability in a-IGZO TFTs was explored by combining the current–voltage (I–V) measurements in double-sweeping V_{GS} mode and capacitance–voltage (C–V) measurements. The NBIS-induced hysteresis was quantitatively analyzed using a positive gate pulse mode. The I–V and C–V results revealed that the trapped holes at the etch-stopper/IGZO interface, the trapped holes at the IGZO/gate insulator interface, and the generation of donor-like states in a-IGZO layer were particularly prominent after NBIS tests when the active layer thickness was close to the Debye length.

Experimental

A schematic cross-sectional view of a bottom-gate a-IGZO TFT is shown in Figure 1a. The detailed fabrication procedure for the a-IGZO TFT was described in our previous publication [24]. After the fabrications of a chromium (Cr) gate electrode and a SiO_x gate insulator (150 nm), the a-IGZO layer with thicknesses of 25, 45, 75, and 100 nm respectively were deposited at 160 °C from a sintered IGZO ceramic target by DC magnetron sputtering with a mixed gas of Ar/O_2 = 29.4/0.6 sccm at a deposition pressure of 1 Pa. After patterning of the IGZO films as the active channel, a SiO_x etch-stopper (200 nm), source and drain electrodes, and a 200 nm-thick SiO_x passivation layer were sequentially formed. Following the preparation of a-IGZO TFTs, all devices were annealed in N_2 environment at 350 °C for 1 h before the electrical measurements. The channel width (W) and length (L) of the IGZO TFTs were 50 and 20 μm, respectively. All of the I–V characteristics were measured using an Agilent 4156C precision semiconductor parameter analyzer.

For the photoleakage current test, monochromatic light irradiation was supplied by a Xe lamp with a band pass filter (FWHM of 10 nm) at an intensity of 0.2 mW/cm^2. The wavelength of the light was in the range of 400–530 nm and was introduced to the

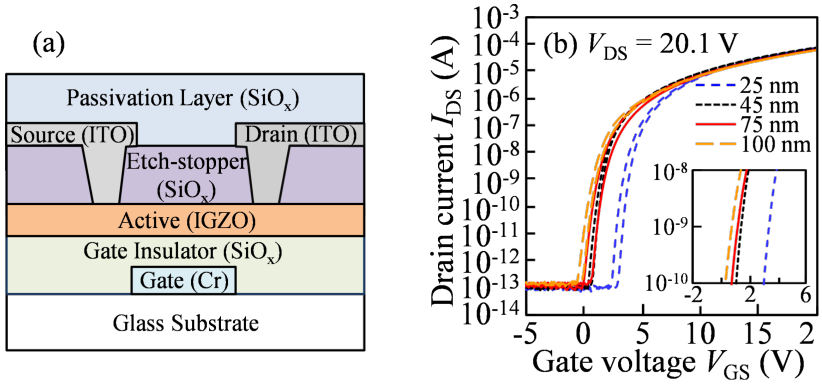

Figure 1: (a) Schematic cross-sectional view and (b) the initial transfer characteristics of a-IGZO TFTs with various active layer thicknesses (T_{IGZO}) measured at V_{DS} = 20.1 V.

back-channel side of a-IGZO TFTs. For the NBIS test, blue light with a wavelength of 460 nm and a gate voltage (V_{GS}) of −30 V was simultaneously applied to all devices during the stress test. The NBIS was interrupted briefly when the transfer characteristics were measured in double-sweeping V_{GS} mode in darkness at V_{DS} = 0.1 V, and then NBIS was reapplied up to a stress time of 10^4 s. In terms of the double-sweeping V_{GS} mode, the transfer characteristics were measured with V_{GS} = −10–20 V (denoted hereafter as forward measurement), and then scanned instantly back to −10 V (denoted hereafter as reverse measurement). The *C*–*V* measurements for the channel capacitance were measured at 1 kHz and an AC level of 100 mV. All of the measurements were carried out at room temperature in ambient air.

Results and Discussion

The initial transfer characteristics (I_{DS}–V_{GS}) of a-IGZO TFTs with various active layer thicknesses (T_{IGZO}) measured at V_{DS} = 20.1 V are shown in Figure 1b. Table 1 summarizes the electrical properties, such as field effect mobility in the saturation region (μ_{sat}), threshold voltage V_{th} (V_{GS} at I_{DS} of 1 nA), hysteresis of the transfer curves (the difference of V_{GS} at I_{DS} of 1 pA between the forward and reverse sweeps), subthreshold swing (SS = $dV_{GS}/d\log_{10}(I_{DS})$), and the maximum area density of state (N_t).

Table 1: The initial electrical properties of a-IGZO TFTs with various active layer thicknesses (T_{IGZO}).

Thickness, T_{IGZO} (nm)	25	45	75	100
μ_{sat} ($cm^2 \cdot V^{-1} \cdot s^{-1}$)	13.61	13.47	12.43	12.20
V_{GS} at I_{DS} = 1 nA (V)	3.35	1.24	1.16	0.74
hysteresis ΔV_H (V)	0.47	0.42	0.35	0.30
subthreshold swing (mV/dec.)	264	273	316	352
trap density (10^{11} cm^{-2})	5.06	5.29	6.35	7.24

Compared to a previous publication [25], the electrical properties of a-IGZO TFTs with various T_{IGZO} exhibit the identical tendency. It is suggested that the devices exhibit great repeatability for the same kind of material under the same fabrication process. In addition, the V_{th} results demonstrate that the free carrier numbers in the bulk of the active layer are gradually increased with increasing T_{IGZO}. Moreover, since the fabrication condition for the IGZO films are exactly identical, except the deposition duration, the results suggest that the variation in the SS value mainly originates from the density of defect states in the active layer. Correspondingly, the obtained results indicate that the increase in the N_t majorly stems from the increase of the IGZO bulk traps because of the identical a-IGZO/GI interfaces.

Figure 2a–d shows the variation in the transfer characteristics of a-IGZO TFTs with various T_{IGZO} under monochromatic light irradiation at the excitation wavelengths of 400, 430, 460, 490, and 530 nm. The transfer characteristics measured in the dark are also shown as a reference. The transfer characteristics of all devices are measured with a V_{DS} of 10.1 V and a V_{GS} scanned from the on-to-off direction. It is found that the photoleakage

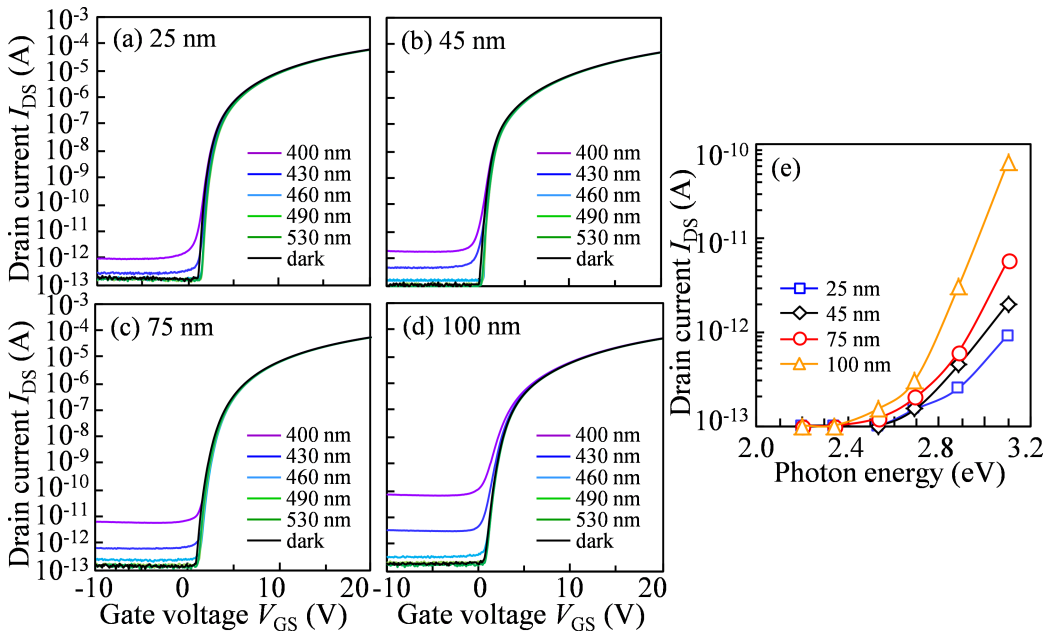

Figure 2: Variation in the transfer characteristics of a-IGZO TFTs with (a) T_{IGZO} = 25, (b) 45, (c) 75, and (d) 100 nm under monochromatic light irradiation, and (e) photoleakage current (V_{GS} = −10 V and V_{DS} = 10 V) of a-IGZO TFTs with various thicknesses as a function of photon energy of the incident light.

current increases in all TFTs when the irradiation wavelength is shorter than 460 nm. In addition, the photoleakage current increases with increasing T_{IGZO}. Figure 2e exhibits the photoleakage current of a-IGZO TFTs with various T_{IGZO} as a function of the photon energy of incident light. When the photon energy exceeds ≈2.7 eV (460 nm), the photoleakage current starts to increase and increases gradually with increasing photon energy. Note that the photoleakage current increases dramatically in the photon energy range of >2.7 eV for the TFT with the thicker T_{IGZO}. These results indicate that the electrons are excited from the trapped states existing near the valence band (E_V) to the conduction band (E_C) even though the photon energy is smaller than the band gap of IGZO. In terms of the a-IGZO material, the high-density electron traps exist at ($E_C - E$) of over 2.7 eV [9], which affect the photoleakage current of a-IGZO TFTs. The total amount of trapped electrons increase with an increase in the T_{IGZO}. The oxygen-related defects, such as oxygen vacancies (V_O), may be the origin of high-density electron traps near the E_V in a-IGZO TFTs, which occupy the region near the valence band maximum with an energy width of ≈1.5 eV [26,27].

Figure 3a–d shows the variation in the transfer characteristics of a-IGZO TFTs with various T_{IGZO} under NBIS for the forward measurements. It is found that for the NBIS duration of 1000 s, the transfer curves of all TFTs shift in the negative V_{GS} direction without SS degradation. When the NBIS duration exceeds 1000 s, a shift in the positive V_{GS} direction as well as the appearance of a hump with SS degradation in the transfer curves is observed, and this phenomenon gradually increases with increasing NBIS duration. It is noted that the phenomenon, combined the positive shift and the hump effect, is weakened as the T_{IGZO} increases. For the reverse measurements, as shown in Figure 3e–h, the transfer curves of all TFTs shift parallel in the positive V_{GS} direction without SS degradation during the NBIS duration of >1000 s. Noticeably, the abnormal phenomenon of hump appearance observed in the forward measurements is hardly observed in the reverse measurements. The positive shift

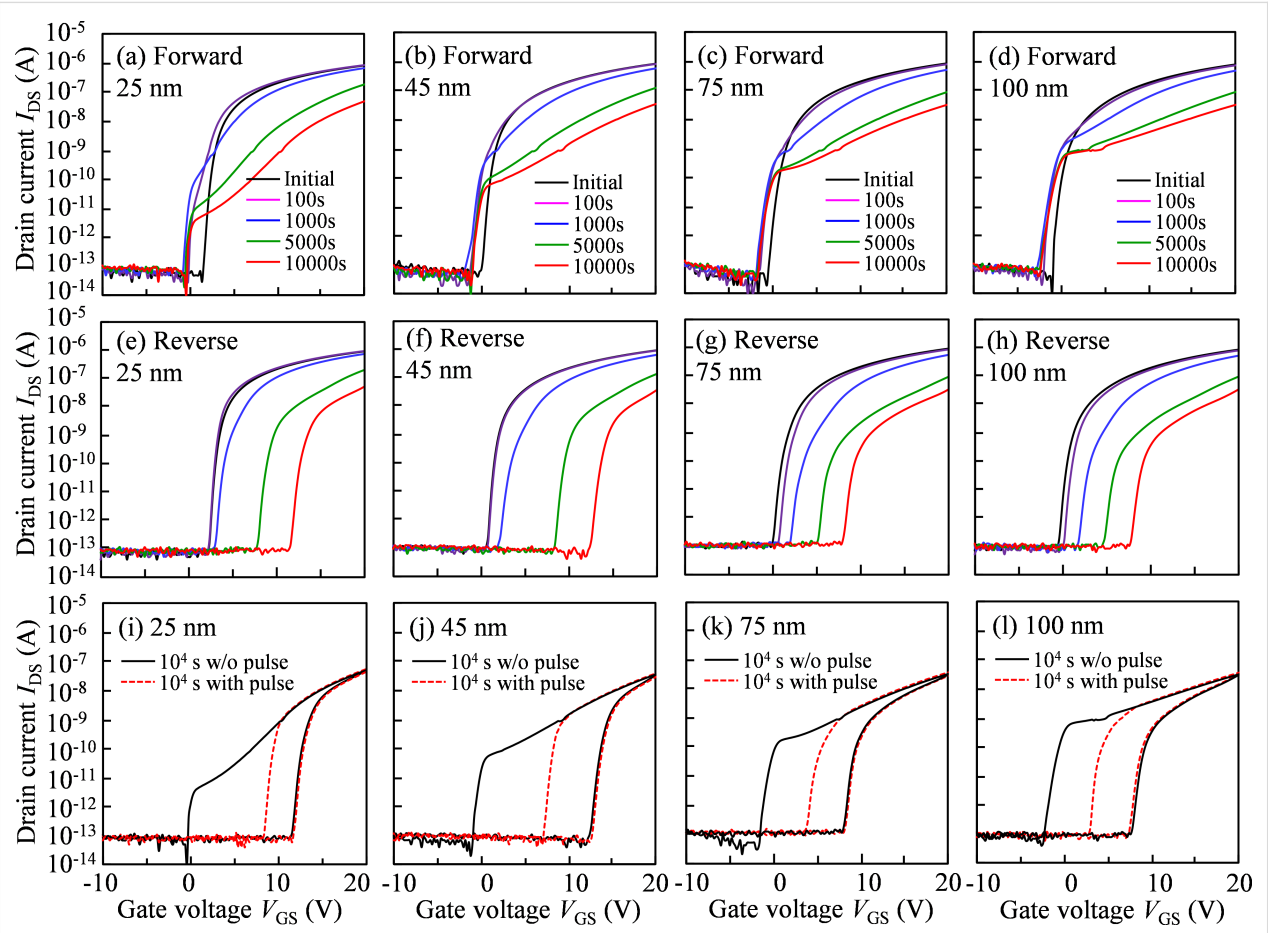

Figure 3: Variation in the transfer characteristics in the forward measurement for a-IGZO TFTs with (a) T_{IGZO} = 25, (b) 45, (c) 75, and (d) 100 nm, and in the reverse measurement with (e) T_{IGZO} = 25, (f) 45, (g) 75, and (h) 100 nm as a function of the stress duration for 10^4 s under −30 V V_{GS} NBIS. Transfer characteristics of a-IGZO TFTs with (i) T_{IGZO} = 25, (j) 45, (k) 75, and (l) 100 nm after 10^4 s NBIS without and with a gate pulse of 1 ms width and 10 V high.

of V_{th} without SS degradation is well fitted to the commonly used stretched-exponential equation [28]. The obtained results suggest that electron trapping at the back-channel interface between a-IGZO and etch-stopper layers occurs because a negative gate bias is performed during NBIS.

On the basis of the photoleakage current results, when the photon energy of the light irradiation exceeds ≈2.7 eV, the photoleakage current of TFTs increases. In this study, a photon energy of ≈2.7 eV is set for the incident light. The previous publication indicates that a photon energy of ≈2.0 and ≈2.3 eV is required for the transition from V_O to V_O^+ and V_O^{2+}, respectively. Moreover, the ionized oxygen vacancies of V_O^+ and V_O^{2+} are located near the mid-gap and the bottom of the E_C [15,29], respectively. It is sufficient to excite high-density V_O defects to V_O^+/V_O^{2+} and then to generate free electrons to E_C. Simultaneously, the electron–hole pairs are photoexcited from E_V, which leads to the neutralization between the ionized V_O^+/V_O^{2+} and the generated electrons, contributing to free holes in E_V [18]. During the NBIS duration with V_{GS} = −30 V, a vertical electric field is exerted along the growth direction of the active layer. In general, the electric potential exponentially declines inside the active layer and has a maximum transfer length called the Debye length. In terms of a-IGZO TFT, a Debye length of ≈40 nm is calculated based on a previous publication [30]. In case of a-IGZO TFT with the T_{IGZO} = 25 nm, the channel layer is totally depleted under the negative V_{GS} bias since the T_{IGZO} is less than the Debye length. Therefore, the photoexcited electrons and holes will be respectively accumulated and trapped at the IGZO/etch-stopper and the GI/IGZO interfaces. Meanwhile, the defect states are generated, which originate from the photoexcited V_O^+/V_O^{2+}. In the forward measurement, the transfer curves exhibit a positive shift in the V_{GS} direction with a hump at the turn-on voltage region when the NBIS duration exceeds 1000 s, which is attributed to the synergistic effects of the generated defect states and the trapped holes at the front-channel interface. After the forward measurement with V_{GS} = −10–20 V, the ionized V_O^+/V_O^{2+} would be gradually neutralized by capturing electrons, and the trapped holes at the front-channel interface are completely de-trapped due to the vertical electric field induced by the positive V_{GS}. Consequently, the abnormal hump observed in the forward measurement disappears in the reverse measurement, suggesting that the donor-like defect states, located near the Fermi level (E_F) at V_{GS} of the turn-on voltage, are generated and stabilized in the IGZO layer. It is noted that the trapped electrons at the back-channel interface are hardly de-trapped even when the positive V_{GS} is applied [17]. As a result, the transfer curves in the reverse measurement exhibit a parallel shift of 10.03 V without SS degradation in the positive V_{GS} direction after the NBIS duration of 10^4 s.

When the T_{IGZO} is increased to 45 nm, which is close to the Debye length, the whole channel layer is almost depleted under the negative V_{GS} bias. During the NBIS duration, more electrons and holes are excited and trapped at the back-channel and the front-channel interfaces. Simultaneously, the high-density defect states are generated due to the increase in the photoexcited V_O^+/V_O^{2+}. As a consequence, after the 10^4 s NBIS duration, the transfer curves show a significant shift in the positive V_{GS} direction with a prominent hump for the forward measurement and display a distinct change of 12.46 V in the positive V_{GS} direction without SS degradation for the reverse measurement, as shown in Figure 4a. When the T_{IGZO} is further increased to 75 and 100 nm, which is larger than the Debye length, the electric potential exponentially decreases inside the active layer under −30 V V_{GS} bias. Although some amount of electrons are photoexcited to E_C, they are partly accumulated and trapped at the back-channel interface due to the weaker vertical electric field. As a result, the excited hole in E_V and the ionized V_O^+/V_O^{2+} near E_F at V_{GS} of the turn-on voltage would be neutralized by the free electrons. Therefore, after the NBIS duration of 10^4 s, the transfer curves exhibit a small shift in the positive V_{GS} direction with a weak hump for the forward measure-

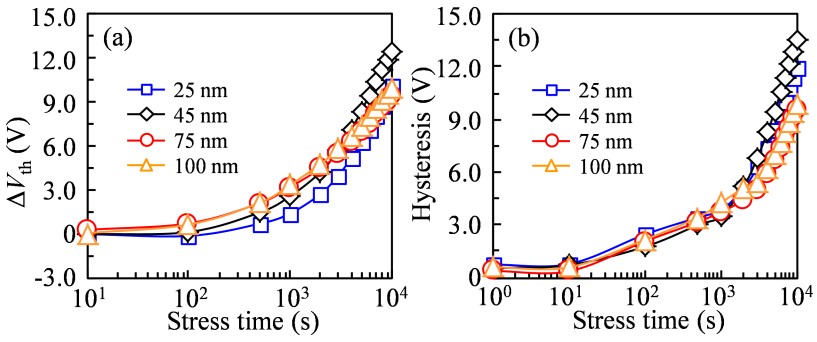

Figure 4: (a) Variation in V_{th} of the transfer curves of a-IGZO TFTs with various T_{IGZO} in the reverse measurement as a function of NBIS duration and (b) hysteresis of a-IGZO TFTs with various T_{IGZO} as a function of NBIS duration.

ment, and show the small shift of 9.45 and 9.96 V in the positive V_{GS} direction for the reverse measurement corresponding to T_{IGZO} = 75 and 100 nm, respectively.

The combination of the transfer curves in the forward and reverse measurements after the NBIS duration of 10^4 s is shown in Figure 4b. The NBIS-induced hysteresis increases remarkably from 11.94 V for the TFT with T_{IGZO} = 25 nm to 13.47 V for the TFT with T_{IGZO} = 45 nm, and decreases drastically to 9.54 and 9.93 V when the T_{IGZO} further increases to 75 and 100 nm. For further quantitative analysis of the origin of the NBIS-induced hysteresis, a positive gate pulse mode is carried out just after the NBIS duration of 10^4 s. Based on our previous publication [17], the optimized condition of a positive gate pulse with pulse width of 1 ms and pulse height of 10 V is enough to neutralize the ionized V_O^+/V_O^{2+}-induced donor-like defect states while it has no influence on the trapped holes at the front-channel interface, as shown in Figure 3i–l. It is found that the trapped hole-induced hysteresis are 3.41, 5.58, 4.39, and 4.62 V corresponding to the IGZO TFTs with T_{IGZO} = 25, 45, 75, and 100 nm, respectively.

To further reveal the mechanism of the NBIS-induced hump and transfer curve shift in a-IGZO TFTs with various T_{IGZO}, *C–V* analyses before and after the NBIS duration of 10^4 s are measured, as shown in Figure 5. In the initial stage, all *C–V* curves without distortion are observed, which are in agreement with the initial *I–V* curves. After the 10^4 s NBIS duration, all *C–V* curves shift in a positive V_{GS} direction with distortion near the turn-on region. The *C–V* results suggest that NBIS-induced defect states are uniform in the whole channel layer near E_F at V_{GS} of the turn-on voltage. In case of a-IGZO TFT with T_{IGZO} = 25 nm, the *C–V* curve shifts 11.4 V in the positive V_{GS} direction with a hump in the off-state. On the basis of the *C–V* results, the energy-band diagrams for the IGZO TFTs with various T_{IGZO} under NBIS are illustrated in Figure 6. The

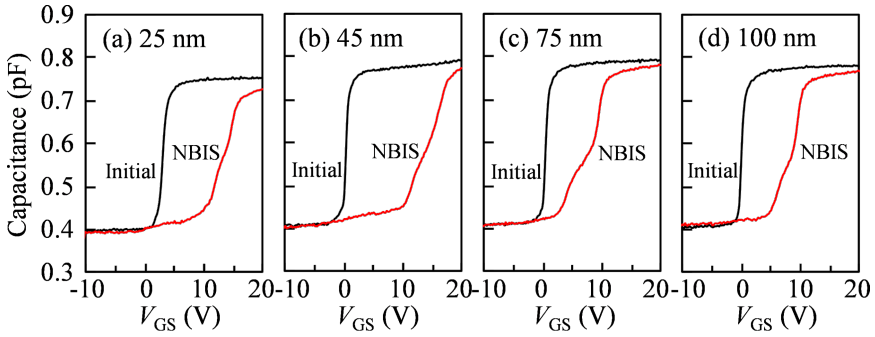

Figure 5: *C–V* curves before and after the NBIS duration of 10^4 s with (a) T_{IGZO} = 25, (b) 45, (c) 75, and (d) 100 nm, respectively.

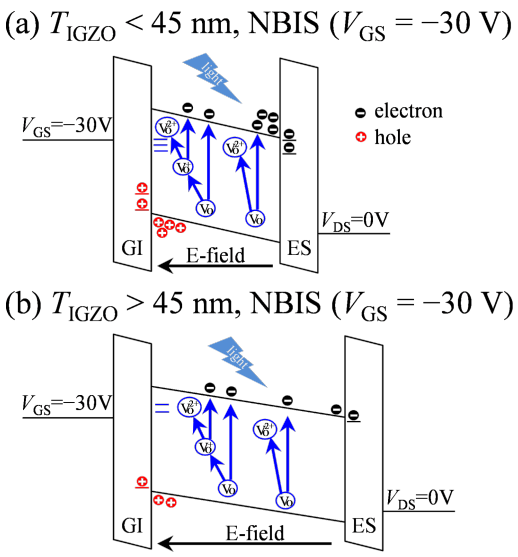

Figure 6: Schematic diagram of NBIS-induced degradation mechanism in a-IGZO TFTs with (a) T_{IGZO} < 45 and (b) over the Debye length (75 and 100 nm).

energy band at the front-channel is remarkably bent upward under the negative V_{GS} bias when the T_{IGZO} is less than the Debye length, as shown in Figure 6a. A hump observed at the turn-on region of the *C–V* curve indicates that the energy level of the generated defect states is located near E_F at V_{GS} of the turn-on voltage. The positive shift of the *C–V* curve demonstrates that electrons are trapped at the back-channel interface due to the vertical electric fields in the channel. When the T_{IGZO} is increased to 45 nm, the *C–V* curve exhibits a large shift of 15.1 V in the positive V_{GS} direction with a distinct hump at the turn-on region. The obtained results suggest that because the T_{IGZO} is close to the Debye length, the high-density defect states are generated in the whole channel layer and more electrons are photoexcited and trapped at the back-channel interface. When the T_{IGZO} is further increased to 75 and 100 nm, the *C–V* curves exhibit smaller shifts of 8.7 and 9.3 V in the positive V_{GS} direction with a weaker hump in the off-state compared to the 45 nm-thick channel layer case. The energy band at the front-channel is slightly bent upward as the T_{IGZO} is much larger than the Debye length, as shown in Figure 6b. The weakened hump near the turn-on region illustrates that the photoexcited V_O^+/V_O^{2+} would be neutralized by the free electrons in E_C, contributing to the low-density defect states near E_F at V_{GS} of turn-on voltage. The small shift of the *C–V* curves demonstrates that the fewer electrons are accumulated and trapped at the back-channel interface. The obtained *C–V* results are correlated with the results of the *I–V* measurements.

On the basis of the above discussion, it is demonstrated that the T_{IGZO} is one of the critical parameters to modify the electrical properties of the device. Besides the active layer thickness, the intrinsic characteristics of a-IGZO and the front- and back-channel interfaces of the TFT also play a vital role for the high-performance devices. Moreover, to reduce the density of oxygen vacancies in the bulk of the IGZO for the enhancement of electrical properties and stress stability of the TFTs, the following two aspects should be mainly considered: (i) oxidizing the densities of the defect state of oxide semiconductors to suppress charge trapping, for example by oxygen annealing and N_2O plasma treatment [31]; and (ii) inactivating the defects in the semiconductor by means of introducing new elements to form stable chemical bonds with the defects, for example by fluoride ion implantation and nitrogen annealing [32,33].

Conclusion

The impact of the T_{IGZO} on the photoleakage current and the NBIS-induced instability in a-IGZO TFTs were systematically investigated. It was found that when the photon energy of the light irradiation exceeds ≈2.7 eV, the photoleakage current increases in all TFTs irrespective of the T_{IGZO} due to the high-density electron traps existing at an ($E_C - E$) of ≈2.7 eV. Because the total amount of trapped electrons increases with increasing T_{IGZO}, the photoleakage current gradually increases with increasing T_{IGZO}. On the basis of the photoleakage current results, the influence of the T_{IGZO} on NBIS with a photon energy of ≈2.7 eV in a-IGZO TFTs is clarified by the *I–V* and *C–V* measurements. In addition, the NBIS-induced hysteresis is quantitatively evaluated through a positive gate pulse mode, contributing to the separation of the trapped holes at the front-channel interface and the generation of donor-like defect states in a-IGZO layer. The obtained *I–V* and *C–V* results indicate that when the T_{IGZO} is close to the Debye length, the trapped holes at the front-channel interface, the trapped electrons at the back-channel interface, and the generated donor-like defect states in a-IGZO are distinctly prominent during NBIS. This study suggests that to improve the reliability of oxide TFTs under light irradiation and gate bias stresses, the quality of the active layer and interface engineering should be taken into account.

Acknowledgements

The authors acknowledge all support from the National Key Research and Development Program of China (2016YFA0202403), the National Nature Science Foundation of China (61674098, 91733301), the Natural Science Foundation of Shaanxi Provincial Department of Education (2017KW-023, 2017JM6020), the Fundamental Research Funds for the Central Universities (GK201603053, GK201702003, GK201601010), the Changjiang Scholar and the Innovative Research Team (IRT_14R33), the 111 Project (B14041), and the Chinese National 1000-talent-plan program (Grant No. 111001034). This work was partly supported by JSPS KAKENHI Grant Number 16K06309.

ORCID® iDs

Dapeng Wang - https://orcid.org/0000-0001-9897-0627
Mamoru Furuta - https://orcid.org/0000-0003-1685-3246

References

1. Nomura, K.; Ohta, H.; Takagi, A.; Kamiya, T.; Hirano, M.; Hosono, H. *Nature* **2004,** *432,* 488–492. doi:10.1038/nature03090
2. Zhang, J.; Yang, J.; Li, Y.; Wilson, J.; Ma, X.; Xin, Q.; Song, A. *Materials* **2017,** *10,* 319. doi:10.3390/ma10030319
3. Hirao, T.; Furuta, M.; Hiramatsu, T.; Matsuda, T.; Li, C.; Furuta, H.; Hokari, H.; Yoshida, M.; Ishii, H.; Kakegawa, M. *IEEE Trans. Electron Devices* **2008,** *55,* 3136–3142. doi:10.1109/ted.2008.2003330
4. Tsai, C.-T.; Chang, T.-C.; Chen, S.-C.; Lo, I.; Tsao, S.-W.; Hung, M.-C.; Chang, J.-J.; Wu, C.-Y.; Huang, C.-Y. *Appl. Phys. Lett.* **2010,** *96,* 242105. doi:10.1063/1.3453870
5. Kim, K. S.; Ahn, C. H.; Kang, W. J.; Cho, S. W.; Jung, S. H.; Yoon, D. H.; Cho, H. K. *Materials* **2017,** *10,* 530. doi:10.3390/ma10050530

6. Liu, A.; Liu, G.; Zhu, C.; Zhu, H.; Fortunato, E.; Martins, R.; Shan, F. *Adv. Electron. Mater.* **2016,** *2,* 1600140. doi:10.1002/aelm.201600140
7. Kim, Y. G.; Kim, T.; Avis, C.; Lee, S.-H.; Jang, J. *IEEE Trans. Electron Devices* **2016,** *63,* 1078–1084. doi:10.1109/ted.2016.2518703
8. Liu, X.; Jiang, L.; Zou, X.; Xiao, X.; Guo, S.; Jiang, C.; Liu, X.; Fan, Z.; Hu, W.; Chen, X.; Lu, W.; Hu, W.; Liao, L. *Adv. Mater.* **2014,** *26,* 2919–2924. doi:10.1002/adma.201305073
9. Shimakawa, S.-i.; Kamada, Y.; Kawaharamura, T.; Wang, D.; Li, C.; Fujita, S.; Hirao, T.; Furuta, M. *Jpn. J. Appl. Phys.* **2012,** *51,* 03CB04. doi:10.7567/jjap.51.03cb04
10. Shimakawa, S.-i.; Wang, D.; Furuta, M. *Jpn. J. Appl. Phys.* **2012,** *51,* 108003. doi:10.7567/jjap.51.108003
11. Chang, Y.-G.; Moon, T.-W.; Kim, D.-H.; Lee, H. S.; Kim, J. H.; Park, K.-s.; Kim, C.-D.; Im, S. *IEEE Electron Device Lett.* **2011,** *32,* 1704–1706. doi:10.1109/led.2011.2167736
12. Oh, H.; Yoon, S.-M.; Ryu, M. K.; Hwang, C.-S.; Yang, S.; Park, S.-H. K. *Appl. Phys. Lett.* **2011,** *98,* 033504. doi:10.1063/1.3540500
13. Kim, B.; Chong, E.; Hyung Kim, D.; Woo Jeon, Y.; Hwan Kim, D.; Yeol Lee, S. *Appl. Phys. Lett.* **2011,** *99,* 062108. doi:10.1063/1.3615304
14. Chen, T. C.; Chang, T. C.; Hsieh, T. Y.; Tsai, C. T.; Chen, S. C.; Lin, C. S.; Jian, F. Y.; Tsai, M. Y. *Thin Solid Films* **2011,** *520,* 1422–1426. doi:10.1016/j.tsf.2011.09.002
15. Oh, H.; Yoon, S.-M.; Ryu, M. K.; Hwang, C.-S.; Yang, S.; Park, S.-H. K. *Appl. Phys. Lett.* **2010,** *97,* 183502. doi:10.1063/1.3510471
16. Huang, S.-Y.; Chang, T.-C.; Lin, L.-W.; Yang, M.-C.; Chen, M.-C.; Jhu, J.-C.; Jian, F.-Y. *Appl. Phys. Lett.* **2012,** *100,* 222901. doi:10.1063/1.4722787
17. Wang, D.; Hung, M. P.; Jiang, J.; Toda, T.; Furuta, M. *ACS Appl. Mater. Interfaces* **2014,** *6,* 5713–5718. doi:10.1021/am500300g
18. Hung, M. P.; Wang, D.; Jiang, J.; Furuta, M. *ECS Solid State Lett.* **2014,** *3,* Q13–Q16. doi:10.1149/2.010403ssl
19. Park, H.-W.; Park, K.; Kwon, J.-Y.; Choi, D.; Chung, K.-B. *IEEE Trans. Electron Devices* **2017,** *64,* 159–163. doi:10.1109/ted.2016.2630043
20. Park, J.; Kim, Y. S.; Kim, J. H.; Park, K.; Park, Y. C.; Kim, H.-S. *J. Alloys Compd.* **2016,** *688,* 666–671. doi:10.1016/j.jallcom.2016.07.245
21. Yang, Z.; Yang, J.; Meng, T.; Qu, M.; Zhang, Q. *Mater. Lett.* **2016,** *166,* 46–50. doi:10.1016/j.matlet.2015.12.029
22. Avis, C.; Hwang, H. R.; Jang, J. *ACS Appl. Mater. Interfaces* **2014,** *6,* 10941–10945. doi:10.1021/am501153w
23. Jeong, J.; Hong, Y. *IEEE Trans. Electron Devices* **2012,** *59,* 710–714. doi:10.1109/ted.2011.2180908
24. Wang, D.; Hung, M. P.; Jiang, J.; Toda, T.; Li, C.; Furuta, M. *Jpn. J. Appl. Phys.* **2014,** *53,* 03CC01. doi:10.7567/jjap.53.03cc01
25. Wang, D.; Zhao, W.; Li, H.; Furuta, M. *Materials* **2018,** *11,* 559. doi:10.3390/ma11040559
26. Nomura, K.; Kamiya, T.; Yanagi, H.; Ikenaga, E.; Yang, K.; Kobayashi, K.; Hirano, M.; Hosono, H. *Appl. Phys. Lett.* **2008,** *92,* 202117. doi:10.1063/1.2927306
27. Kamiya, T.; Nomura, K.; Hosono, H. *J. Disp. Technol.* **2009,** *5,* 468–483. doi:10.1109/jdt.2009.2034559
28. Libsch, F. R.; Kanicki, J. *Appl. Phys. Lett.* **1993,** *62,* 1286–1288. doi:10.1063/1.108709
29. Janotti, A.; Van de Walle, C. G. *Appl. Phys. Lett.* **2005,** *87,* 122102. doi:10.1063/1.2053360
30. Li, Y.; Pei, Y. L.; Hu, R. Q.; Chen, Z. M.; Zhao, Y.; Shen, Z.; Fan, B. F.; Liang, J.; Wang, G. *Curr. Appl. Phys.* **2014,** *14,* 941–945. doi:10.1016/j.cap.2014.04.011
31. Chang, G.-W.; Chang, T.-C.; Jhu, J.-C.; Tsai, T.-M.; Syu, Y.-E.; Chang, K.-C.; Tai, Y.-H.; Jian, F.-Y.; Hung, Y.-C. *Appl. Phys. Lett.* **2012,** *100,* 182103. doi:10.1063/1.4709417
32. Wang, D.; Jiang, J.; Furuta, M. *J. Disp. Technol.* **2016,** *12,* 258–262. doi:10.1109/jdt.2015.2472981
33. Yoon, S.; Tak, Y. J.; Yoon, D. H.; Choi, U. H.; Park, J.-S.; Ahn, B. D.; Kim, H. J. *ACS Appl. Mater. Interfaces* **2014,** *6,* 13496–13501. doi:10.1021/am502571w

License and Terms

This is an Open Access article under the terms of the Creative Commons Attribution License (http://creativecommons.org/licenses/by/4.0). Please note that the reuse, redistribution and reproduction in particular requires that the authors and source are credited.

The license is subject to the *Beilstein Journal of Nanotechnology* terms and conditions: (https://www.beilstein-journals.org/bjnano)

The definitive version of this article is the electronic one which can be found at: doi:10.3762/bjnano.9.239